

Universal Nonequilibrium I - V Curve at an Interacting Impurity Quantum Critical Point

Gu Zhang,¹ Chung-Hou Chung,^{2,3,*} Chung-Ting Ke,¹ Chao-Yun Lin,² Henok Mebrahtu,¹
Alex I. Smirnov,⁴ Gleb Finkelstein,^{1,†} and Harold U. Baranger^{1,‡}

¹Department of Physics, Duke University, Durham, North Carolina 27708-0305, U.S.A.

²Department of Electrophysics, National Chiao-Tung University, HsinChu, Taiwan, R.O.C.

³Physics Division, National Center for Theoretical Sciences, HsinChu, Taiwan, R.O.C.

⁴Department of Chemistry, North Carolina State University, Raleigh, North Carolina 27695, U.S.A.

(Dated: 23 September 2018)

Nonequilibrium properties of correlated quantum matter are being intensively investigated because of the rich interplay between the external drive and the many-body correlations. Of particular interest is the nonequilibrium behavior near a quantum critical point (QCP), where the system is delicately balanced between different ground states. Although such effects are typically out of reach, we meet this challenge, providing here both both an analytical calculation of the nonequilibrium I - V curve when the system is tuned to be critical and experimental results to which the theory is compared. The system is a quantum dot coupled to resistive leads: a spinless resonant level interacting with an ohmic dissipative environment. A two-channel Kondo QCP occurs when the level is on resonance and symmetrically coupled to the leads. Using a bosonized representation, we calculate the nonlinear I - V curve at the critical value of the gate voltage corresponding to this QCP. We then show that it has a physically intuitive interpretation in terms of weak backscattering of non-interacting fermions coupled to a modified environment, thus arriving at the same result through dynamical Coulomb blockade theory. The quantitative agreement between the experimental data and our theory, with no fitting parameter, is remarkable. As our system is fully accessible to both theory and experiment, it provides an ideal setting for addressing nonequilibrium phenomena in correlated quantum matter.

I. INTRODUCTION

Quantum phase transitions (QPT)—abrupt changes of ground state due to quantum fluctuations as a parameter is tuned—are of fundamental importance in a wide variety of condensed matter many-body systems ranging from quantum materials to quantum magnets and nanostructures [1–4]. The quantum critical point (QCP) separating the two competing ground states dominates physical properties even at finite temperature where a quantum critical region exists (see Fig. 1) [1, 2]. By tuning parameters of the system to their critical values, the system stays in the critical region down to zero temperature: the system is tuned to criticality, such as for path 1 in Fig. 1. In contrast, detuning results in a crossover from quantum critical behavior to one of the trivial phases (path 2). Along path 1, it is well established that thermodynamic observables at low temperature show universal scaling. Properties away from equilibrium, such as when a bias is applied (a nonequilibrium steady state) or a parameter suddenly changed (a quantum quench), are much less well understood. Indeed, quantum nonequilibrium phenomena are receiving increasing scrutiny in recent years, and unanticipated features near QPT have come to light [1, 5–7]. Here we present the first theoretical and experimental study of a nonequilibrium I - V curve in a system tuned to criticality.

QPT occur not only in the bulk but also on the boundary of interacting systems, as in quantum impurity models [3]. The two-channel Kondo model is a prototypical example: two independent metallic channels each screen a local-

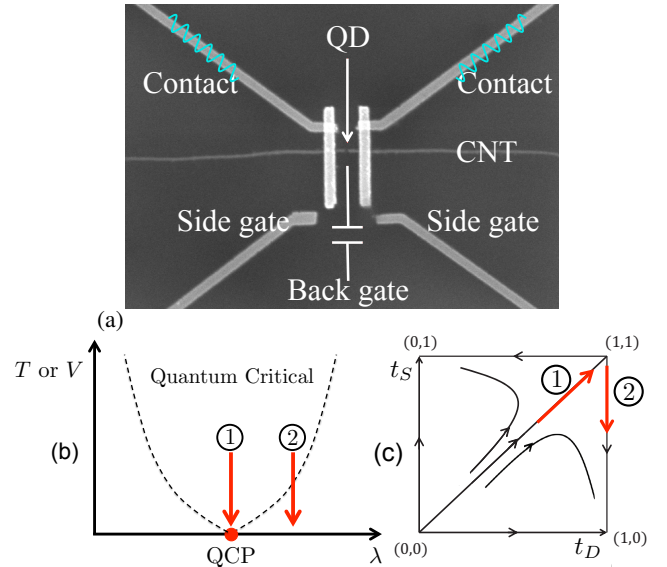


FIG. 1. (a) Schematic of the system overlaid on a SEM image of a sample. A quantum dot is formed in the carbon nanotube (CNT) between the source and drain leads. These resistive leads create a dissipative environment for electrons tunneling through the dot. The tunneling barriers can be tuned with the side gates SG1 and SG2. Applying a bias between the source and drain produces a nonequilibrium steady state. (b) Diagram of a quantum critical region as a function of a system parameter, λ , and temperature or voltage bias. When parameters of the system are tuned to their critical values, the quantum critical region extends down to zero temperature or bias (path 1), otherwise a crossover to one of the trivial ground states occurs (path 2). (c) The RG flow of source and drain coupling (t_S, t_D) when the system is on resonance. For symmetric coupling, the flow is into the strong coupling fixed point (1,1) (path 1) which is the QCP. A slight detuning leads to a crossover to a trivial fixed point (path 2). In this work, we focus exclusively on path 1, which ends at the QCP.

* chung@mail.nctu.edu.tw

† gleb@phy.duke.edu

‡ baranger@phy.duke.edu

ized spin, resulting in frustration and a non-Fermi liquid QCP. Nanoscale systems are ideal for studying impurity QPT because of the exquisite control over parameters that they provide. Indeed, a growing number of QPT are being studied in nanosystems, including e.g. spin [8, 9] and charge [10, 11] two-channel Kondo systems and the $0-\pi$ transition in a Josephson junction [12–14]. These nanosystem QPT can provide insight into more complex quantum impurity QPT, such as those that arise in dynamical mean field theory treatments of strongly correlated materials [6, 15].

Here we present both an analytical calculation of the nonequilibrium I - V curve with system parameters tuned to correspond to a QCP and experimental results to which the theory is compared in detail. The system is a spin-polarized carbon nanotube quantum dot connected to resistive leads via tunable tunnel barriers (Fig. 1). The resistance of the leads creates an ohmic dissipative environment [16–18], and the quantum dot serves as the quantum impurity. The QCP occurs when both (i) a level in the dot is resonant with the leads and (ii) the dot is symmetrically coupled to them. Both of these properties can be fine-tuned using gate voltages. At the QCP, the conductance through the dot at zero temperature becomes perfect (e^2/h when $T \rightarrow 0$), while otherwise it tends to zero. The QCP is of the *two-channel Kondo* type [17]. We previously presented several scaling relations, including non-Fermi liquid scaling along path 1 in Fig. 1, in the equilibrium regime [18].

The interplay between nonequilibrium and many-body effects has been studied in a variety of nanosystems through nonlinear I - V characteristics, both experimentally [12, 19–28] and theoretically [29–46]. Experimental systems studied include, for instance, the Kondo effect in quantum dots, tunneling into edge channels, and dissipative tunneling. However, to our knowledge, the nonequilibrium I - V curve of a system tuned exactly to the critical value of the tuning control parameter corresponding to a QCP has not been measured previously, except for some preliminary indications in our own work [18][47]. Nonlinear I - V curves in the critical regime of a QCP have certainly been reported (for example [8, 9, 13, 48, 49]), but these all involved measurements through weakly coupled leads that therefore probe the density of states in the remainder of the system *in equilibrium*. Such a measurement is called tunneling or transport *spectroscopy* [50], in which no truly nonequilibrium effects are involved [51]. Theoretically, in the scaling regime in which $I \propto V^\alpha$, the exponent α has been frequently deduced from the scaling dimension of the leading operators at the QCP (see for example [52, 53]). With regard to a full calculation beyond the scaling exponent, analytical I - V curves have been obtained for the crossover from a QCP to a Fermi liquid state in the cases of the two-impurity, two-channel, and topological Kondo models [42–45]. In Fig. 1 these correspond to properties along path 2, in which one moves out of the quantum critical region. In contrast, here we are exclusively interested in paths that start or end at the QCP, such as path 1. Somewhat surprisingly, the nonequilibrium I - V characteristics of a system originally tuned to a QCP have not previously been studied either *experimentally* or *theoretically*.

The plan and main results of the paper are as follows. We start by defining our model for the dissipative resonant-level problem (Sec. II) and then immediately bosonize it (Sec. III). In Sec. IV we carry out the key step of obtaining the effective Hamiltonian at strong tunneling, Eq. (15). This then is the model of the QCP.

Resonant tunneling in a Luttinger liquid (LL) provides considerable theoretical guidance in Secs. III and IV because tunneling in a resistive environment is an emulation of that system [17, 18, 26, 54–58]. In equilibrium, resonant peaks of perfect conductance in a LL have been extensively studied theoretically [59–67], and this system has a similar two-channel Kondo QCP, separating single-barrier (left or right) dominated weak-tunneling regimes [60, 65]. There are significant differences in the strong-coupling model (discussed below), however, and furthermore nonequilibrium properties at the LL resonant tunneling QCP have been studied only in the scaling regime (see e.g. [59, 60]).

In Sec. V, we find the I - V characteristics in the quantum critical regime beyond simple scaling. We start from a Keldysh approach, which then reduces to finding backscattering rates from the golden rule. This simplification is possible because we work to second order in the backscattering amplitude (but to all orders in the coupling to the environment). The main theoretical result of the paper is the analytical expression for the nonlinear I - V curve at finite temperature, Eq. (21).

Experimental results are presented in Sec. VI and compared with the theory. In particular, Fig. 2 shows excellent agreement between theory and experiment.

Before concluding, we then show in Sec. VII that this result has a simple physical interpretation, one that is not available in the corresponding LL problem. Here, modes that initially do not couple to the environment map to *non-interacting* left-moving and right-moving fermions. Indeed, near the QCP the natural degrees of freedom are right-moving and left-moving fermionic channels between which there is weak tunneling in a modified environment. In this form, dynamical Coulomb blockade theory [68–70] yields the same expression for the I - V curve as in Sec. V.

II. MODEL AND HAMILTONIAN

Our system is shown in Fig. 1: a spinless resonant level between two resistive leads. The Hamiltonian in the weak-tunneling regime consists of several parts,

$$H = H_{\text{Dot}} + H_{\text{Leads}} + H_\mu + H_T + H_{\text{Env}}. \quad (1)$$

$H_{\text{Dot}} = \epsilon_d d^\dagger d$ models the dot with single energy level ϵ_d , which may be tuned by the backgate voltage V_{gate} .

$$H_{\text{Leads}} = \sum_{\alpha=S,D} \sum_k \epsilon_k c_{k\alpha}^\dagger c_{k\alpha} \quad (2)$$

represents the electrons in the source (S) and drain (D) leads, and

$$H_\mu = \sum_{\alpha=S,D} \sum_k \mu_\alpha c_{k\alpha}^\dagger c_{k\alpha} \quad (3)$$

is the chemical potential term driving the system out of equilibrium through the applied bias V , $\mu_{S/D} = \pm V/2$.

Tunneling in our system excites the resistive environment through fluctuations of the voltage on the source and drain. These require a quantum description of the tunnel junction [68–71] via junction charge and phase fluctuation operators that are conjugate to each other, $\varphi_{S/D}$ and $Q_{S/D}$. A tunneling event shifts the charge on the corresponding junction, as, for example, in this contribution to tunneling from the dot to the source: $c_{kS}^\dagger e^{-i\sqrt{2\pi}\varphi_S} d$. We take the capacitance of the two tunnel junctions to be the same and so it is natural to consider the sum and difference variables $\psi \equiv (\varphi_S + \varphi_D)/2$ and $\varphi \equiv \varphi_S - \varphi_D$. The fluctuations φ involve charge flow through the system and so couple to the environment. In contrast, ψ is related to the total charge in the dot. Since the total charge is not coupled to the environment [68, 69, 72], we drop ψ at this point. We thus arrive at the tunnel Hamiltonian

$$H_T = \sum_k \left(t_S c_{kS}^\dagger e^{-i\sqrt{\frac{\pi}{2}}\varphi} d + t_D c_{kD}^\dagger e^{i\sqrt{\frac{\pi}{2}}\varphi} d + \text{h.c.} \right). \quad (4)$$

Because of the sum over momentum, only the fields at $x = 0$ couple to the dot and environment. Since the parameters t_S and t_D are initially small, the system starts in the weak coupling regime.

Finally, the ohmic environment of resistance R is modeled in the usual way as a bath of harmonic oscillators to which the phase fluctuations φ of the junction are coupled. The model must produce the expected temporal correlations of the phase fluctuations, namely $\langle e^{-i\varphi(t)} e^{i\varphi(0)} \rangle \propto (1/t)^{2r}$ where the exponent r is related to the resistance of the environment by $r \equiv Re^2/h$ [68–71]. We choose to represent the environment by bosonic fields $\varphi(x)$ and its conjugate $\vartheta(x)$ with Hamiltonian

$$H_{\text{Env}} = \frac{1}{2} \int_0^\infty dx \left[\frac{1}{2r} (\partial_x \varphi)^2 + 2r (\partial_x \vartheta)^2 \right], \quad (5)$$

which is coupled to the junction by identifying $\varphi(x=0)$ as the phase φ in Eq. (4).

III. BOSONIZATION AT WEAK COUPLING

Our strategy is to develop a bosonized form of the weak-coupling Hamiltonian. Bosonization is possible because an impurity couples to only an effectively one-dimensional (1D) subset of lead states (for non-interacting electrons). We label these semi-infinite 1D leads $x \in (-\infty, 0)$ for S and $x \in (0, +\infty)$ for D (and set their Fermi velocities equal to one).

We bosonize in the standard way [59, 73], choosing the conventions of Ref. [59]:

$$c_{\alpha,L/R}^\dagger(x,t) = e^{\pm ik_F x} \frac{F_\alpha}{\sqrt{2\pi a_0}} e^{i\sqrt{\pi}[\phi_\alpha(x,t) \pm \theta_\alpha(x,t)]} \quad (6)$$

where $\alpha = S/D$ and L/R (\pm in the exponents) indicates left- or right-moving particles. ϕ_α and θ_α are conjugate bosonic operators that describe electronic states in the semi-infinite leads, obeying the standard commutation relation $[\phi(x'), \partial_x \theta(x)] = i\pi \delta(x' - x)$. a_0 is a short time cutoff, and the F_α are Klein factors. In bosonic form, the electron density is $\rho_{L/R}(x) = [\pm \partial_x \phi(x) + \partial_x \theta(x) + k_F/\sqrt{\pi}]/(2\sqrt{\pi})$. It is convenient to form the charge and flavor fields [30],

$$\begin{aligned} \phi_{f/c}(x) &\equiv \frac{1}{2} [\phi_S(-x) \mp \phi_D(x) \pm \theta_S(-x) - \theta_D(x)] \\ \theta_{c/f}(x) &\equiv \frac{1}{2} [\pm \phi_S(-x) + \phi_D(x) + \theta_S(-x) \pm \theta_D(x)]. \end{aligned} \quad (7)$$

Note that $\phi_f(x)$ is conjugate to $\theta_c(x)$ and likewise $\phi_c(x)$ to $\theta_f(x)$.

The voltage bias in H_μ is handled using a time-dependent gauge transformation [59, 68] that moves the bias to the tunneling term—physically, when an electron hops from a lead to the dot it acquires a phase factor corresponding to the drop in bias (change in energy) across that barrier. Since the QCP occurs at symmetric coupling, we take identical coupling to the source and drain leads, $t_S = t_D \equiv t$. With symmetric tunneling and capacitance, the bias voltage drops symmetrically as well. The tunneling term is, then,

$$\begin{aligned} H_{T+\mu} &= \frac{t}{\sqrt{2\pi a_0}} \left[F_S d e^{i\sqrt{\pi}\phi_c} e^{i(\sqrt{\pi}\phi_f - \sqrt{\frac{\pi}{2}}\varphi + eVt/2)} \right. \\ &\quad \left. + F_D d e^{i\sqrt{\pi}\phi_c} e^{-i(\sqrt{\pi}\phi_f - \sqrt{\frac{\pi}{2}}\varphi + eVt/2)} + \text{h.c.} \right]. \end{aligned} \quad (8)$$

All fields in Eq. (8) are taken at $x = 0$, and we have used $\theta_{S/D}(0) = 0$ [59, 74] due to the Dirichlet boundary condition at the end of the leads.

Notice that the fields $\phi_f(x=0)$ and φ enter in the same way in Eq. (8), so it is natural to combine them via

$$\begin{aligned} \phi'_f(x) &= \phi_f(x) - \frac{1}{\sqrt{2}} \varphi(x) \\ \varphi'(x) &= \sqrt{r} \phi_f(x) + \frac{1}{\sqrt{2r}} \varphi(x). \end{aligned} \quad (9)$$

Since the field φ' completely decouples from the problem, we drop it from further consideration. The final expression for the Hamiltonian at weak coupling is

$$\begin{aligned} H_{\text{Leads+Env}}^{\text{eff}} + H_{\text{Dot}} &= \frac{1}{2} \int_0^\infty dx \left[(\partial_x \theta_f)^2 + (\partial_x \phi_c)^2 + (1+r)(\partial_x \theta'_c)^2 + \frac{1}{1+r} (\partial_x \phi'_f)^2 \right] + \epsilon_d d^\dagger d \\ H_{T+\mu} &= \frac{t}{\sqrt{2\pi a_0}} \left\{ F_S d e^{i\sqrt{\pi}\phi_c} e^{i(\sqrt{\pi}\phi'_f + eVt/2)} + F_D d e^{i\sqrt{\pi}\phi_c} e^{-i(\sqrt{\pi}\phi'_f + eVt/2)} + \text{h.c.} \right\}. \end{aligned} \quad (10)$$

Thus we see that the coupling of each tunneling electron to the environment generates an effective interaction between them. Here, *one* of the sets of lead fields, (ϕ'_f, θ'_c) , becomes interacting; in contrast, in a Luttinger liquid, *both* sets of lead fields would be interacting, an important distinction when we come to interpreting our results (see Sec. VII).

When the dot is symmetrically coupled to the leads and is exactly on resonance ($\epsilon_d = 0$), the weak-coupling description above renormalizes to a strong-coupling fixed point [17]. This comes about because of frustration. If the coupling is not symmetric, the fixed point to which the system flows corresponds to cutting the system at the weaker link and incorporating the dot into the other lead [see Fig. 1(c)]. Frustration between incorporating the dot into the source or drain ensues when the coupling is symmetric. As a result, the dot ends up being hybridized with both leads, and the system looks increasingly uniform.

IV. THE STRONG TUNNELING LIMIT: LINK TO A WEAK DOUBLE BARRIER

As the system scales to strong coupling, it approaches a symmetric fixed point at which the system is translationally invariant and so fully transparent. The properties of this fixed point are heavily constrained by its being one of the two possible boundary fixed points in the corresponding conformal field theory (the “periodic” fixed point) [75, 76]. Because of this constraint, the strong coupling fixed point in our dissipative resonant level model is the same as in the Luttinger liquid case [59–61]; indeed, the effect of the total charge field (ϕ_c, θ_f) (which is interacting in a Luttinger liquid but non-interacting here) scales to zero at the fixed point. Furthermore, any model that scales to the strong coupling point can be used to deduce the properties near that point. In particular, a wire with two weak potential barriers is a good model for the residual effect of the quantum dot [59, 64].

For an explicit description of the strong tunneling limit that allows calculation of the I - V curve, we therefore start with two symmetric δ -function barriers spaced by ℓ in a 1D wire of fermions denoted $\psi_R(x)$ and $\psi_L(x)$ for left and right movers. The fermions are then described via bosonization by

the canonical bosonic fields θ and ϕ [59]. For the moment the fields are non-interacting; we add the effect of the environment and the bias later on. The Hamiltonian is $H_0 + H_T$ where

$$H_0 = \frac{1}{2} \int_{-\infty}^{\infty} dx [(\partial_x \theta)^2 + (\partial_x \phi)^2], \quad (11a)$$

$$H_T = A \sum_{\pm} \cos[2\sqrt{\pi}\theta(\pm\ell/2) \pm k_F \ell]. \quad (11b)$$

The form $\cos[2\sqrt{\pi}\theta]$ appears because it corresponds to $2k_F$ backscattering of the underlying fermions [59], $\psi_R^\dagger \psi_L + \text{h.c.}$, as can be checked by using the bosonization relation Eq. (6) for $\psi_{L,R}$ to refermionize this term. This is, of course, the expected effect of scattering from a potential barrier.

As in the weak barrier case, it is convenient to form the sum and difference fields

$$\theta_c \equiv [\theta(\ell/2) + \theta(-\ell/2)]/2 \text{ and } \theta_f \equiv [\theta(\ell/2) - \theta(-\ell/2)]/2. \quad (12)$$

(In contrast to the weak-tunneling case, the ϕ fields now have Dirichlet boundary conditions, becoming discretized constants at strong coupling [59, 74], and so do not appear in the expressions for θ_c and θ_f here.) When on resonance for a single level, one has $k_F \ell = \pi/2$ at strong coupling [73], so that the barrier terms become

$$H_T = A \cos(2\sqrt{\pi}\theta_c) \sin(2\sqrt{\pi}\theta_f). \quad (13)$$

We now incorporate the external bias potential V and the fluctuating potential caused by the environmental field φ . The environmental potential fluctuations are given by $\sqrt{2\pi}\dot{\varphi}$ which in a Hamiltonian formulation corresponds to $ir2\sqrt{2\pi}\partial_x\vartheta(0)$, where $\partial_x\vartheta(0)$ appears naturally as the charge fluctuation operator conjugate to φ [see Eq. (5)]. Though at weak coupling this potential difference is applied between the source and drain leads, Eq. (3), at strong coupling, in contrast, the potential is applied between the right-moving fermions (those coming from the source) and left-moving fermions (from the drain). Applying the potential in this way is commonly done, for instance, in discussing the quantum Hall effect [50]. Thus, in terms of the strong coupling fermions $\psi_R(x)$ and $\psi_L(x)$ the bias and environmental coupling are

$$H_{\mu+\text{Env}} = \frac{eV + ir2\sqrt{2\pi}\partial_x\vartheta(0)}{2} \left[\int_{-\infty}^{-\ell/2} dx \psi_R^\dagger(x)\psi_R(x) - \int_{\ell/2}^{\infty} dx \psi_L^\dagger(x)\psi_L(x) \right] \quad (14a)$$

$$= \frac{eV + ir2\sqrt{2\pi}\partial_x\vartheta(0)}{4} \frac{1}{\sqrt{\pi}} \left[\int_{-\infty}^{-\ell/2} dx [\partial_x \theta(x) - \partial_x \phi(x)] - \int_{\ell/2}^{\infty} dx [\partial_x \theta(x) + \partial_x \phi(x)] \right] \quad (14b)$$

$$= - \left[\frac{eV}{4\sqrt{\pi}} + i2\sqrt{2r}\partial_x\vartheta(0) \right] \int_0^{\infty} dx \partial_x \theta_c(x). \quad (14c)$$

The dependence on bias, the first term in (14c), is handled by performing a time-dependent gauge transformation that

moves the bias into the barrier term H_T , as at weak coupling. Thus, in Eq. (13) $\cos(2\sqrt{\pi}\theta_c) \rightarrow \cos(2\sqrt{\pi}\theta_c + eVt)$.

Since the right-moving particles (from the source) have chemical potential eV higher than that of the left-moving particles (from the drain), it is natural that the bias appears as a phase eVt in the backscattering operator.

The next step is to integrate out the environmental degrees of freedom $\vartheta(x)$ and $\varphi(x)$. The bilinear coupling to the lead fermions, the second term in (14c), then generates an effective coupling that causes $\theta_c(x)$ and $\phi_f(x)$ to be interacting fields. The integrating-out procedure is best performed in a Lagrangian formulation and is outlined in Appendix A. Since they are interacting fields, we relabel them θ'_c and ϕ'_f for consistency. Indeed, the resulting free Hamiltonian is, as expected, identical to that at weak coupling, Eq. (10).

The strong-coupling effective model thus obtained is

$$H^{\text{eff}} = \frac{1}{2} \int_0^\infty dx \left[(\partial_x \theta_f)^2 + (\partial_x \phi_c)^2 \right] \quad (15a)$$

$$+ (1+r)(\partial_x \theta'_c)^2 + \frac{1}{1+r} (\partial_x \phi'_f)^2 \quad (15b)$$

$$+ A \cos [2\sqrt{\pi}\theta'_c(0) + eVt] \sin [2\sqrt{\pi}\theta_f(0)]. \quad (15c)$$

We emphasize that the modes represented by fields θ_f and ϕ_c are free while those represented by θ'_c and ϕ'_f are interacting [77]. The coupling between these two sets of modes is given by the barrier term, (15c), that describes the deviation from the uniform state characterizing the QCP. Recalling that a bosonic operator of the form $\cos(2\sqrt{\pi}\theta)$ corresponds to backscattering of the underlying fermions, we see that this coupling involves the *simultaneous* backscattering of both sets of modes. Note that the bias enters the backscattering of the interacting modes.

The strength of the barrier term, A , is not known microscopically as it is the result of the flow from weak to strong coupling. It is helpful to recall at this point the equilibrium flow to the strong coupling point. The equilibrium RG scaling equation for A coming from Eq. (15c) is

$$\frac{dA}{d \ln D} = \frac{1}{1+r} A, \quad (16)$$

where the energy cutoff D runs from $D_0 = 1$ down to 0—see the supplementary material for an explicit demonstration using standard methods [78]. The scaling dimension of the backscattering operator is then $\Omega \equiv 1 + 1/(1+r)$, showing that the operator is irrelevant and $A \rightarrow 0$ at the QCP.

The linear response conductance at zero temperature is thus that of the system defined by Eqs. (15a)-(15b). By combining the charge and flavor fields, one clearly obtains a translationally invariant system (for details see [79]), in which one therefore has perfect transmission and thus $G = e^2/h$ [17]. This is the same result as for resonant tunneling in a Luttinger liquid [59, 60]; in fact, the scaling dimension of the backscattering operator here is also the same. This connection is explained

explicitly in Appendix B. From general considerations (see, e.g., [60]) one expects the low temperature or bias deviation from perfect transmission to be a power law related to this scaling dimension, namely $|dI/dV - e^2/h| \propto T^{2/(1+r)}$ or $\propto V^{2/(1+r)}$.

V. THE I - V CURVE

We now turn to an explicit calculation of the I - V curve: we find the correction to perfect transmission caused by the joint backscattering term Eq. (15c). Because A is small, we work to leading order in this term but keep all orders in the bosonic fields, and use a Keldysh approach to find the nonequilibrium current [80]. The fact that we work to only second order in A leads to a considerable simplification [81, 82]: a Keldysh calculation for scattering by a local operator to second order shows that the current is related to the backscattering rate $\Gamma(V, T)$, which in turn is given simply by a golden rule expression [81, 82]. The current is given by the difference between the forward and backward rates; consequently, the backscattering-related current is $\Delta I(V, T) = e[\Gamma(V, T) - \Gamma(-V, T)]$.

The backscattering matrix element needed is [56]

$$\begin{aligned} \langle f | H_T | i \rangle &= A \langle R_1^f | \cos[2\sqrt{\pi}\theta'_c(0)] | R_1^i \rangle \\ &\times \langle R_2^f | \sin[2\sqrt{\pi}\theta_f(0)] | R_2^i \rangle, \end{aligned} \quad (17)$$

where $|R_1\rangle$ and $|R_2\rangle$ represent the states of θ'_c and θ_f , respectively, and i and f label the initial and final states. Recall that in time-dependent perturbation theory, an explicit oscillatory time dependence such as eVt in Eq. (15c) factors out and enters the energy conservation constraint. The rate is, then, given by

$$\begin{aligned} \Gamma(V, T) &= A^2 \frac{2\pi}{\hbar} \sum_{R_1^i R_1^f} \sum_{R_2^i R_2^f} \\ &\times |\langle R_1^f | \cos[2\sqrt{\pi}\theta'_c(0)] | R_1^i \rangle|^2 P_\beta(R_1^i) \\ &\times |\langle R_2^f | \sin[2\sqrt{\pi}\theta_f(0)] | R_2^i \rangle|^2 P_\beta(R_2^i) \\ &\times \delta(E_{R_1^i} + E_{R_2^i} + eV - E_{R_1^f} - E_{R_2^f}), \end{aligned} \quad (18)$$

where $P_\beta(R_{1,2}^i) = \langle R_{1,2}^i | \rho_\beta | R_{1,2}^i \rangle$ refers to the density matrices of the fields and the subscript β is a reminder of the effect of temperature.

To evaluate the rate, first rewrite the δ -function as an integral over time of an exponential. Then, notice that the factors $\exp(iE_{i,f}t/\hbar)$ can be produced by acting on the initial or final state with $\exp(iHt/\hbar)$. Thus, changing to the Heisenberg picture for the fields and dropping the argument $x = 0$ for clarity, we find

$$\begin{aligned}
\Gamma(V, T) &= \frac{A^2}{\hbar^2} \int_{-\infty}^{\infty} dt \sum_{R_1^i R_1^f} \langle R_1^i | \cos [2\sqrt{\pi}\theta'_c(t)] | R_1^f \rangle \langle R_1^f | \cos [2\sqrt{\pi}\theta'_c(t=0)] | R_1^i \rangle P_\beta(R_1^i) \\
&\quad \times \sum_{R_2^i R_2^f} \langle R_2^i | \sin [2\sqrt{\pi}\theta_f(t)] | R_2^f \rangle \langle R_2^f | \sin [2\sqrt{\pi}\theta_f(t=0)] | R_2^i \rangle P_\beta(R_2^i) e^{ieVt/\hbar} \\
&= \frac{A^2}{\hbar^2} \int_{-\infty}^{\infty} dt e^{ieVt/\hbar} \langle \cos [2\sqrt{\pi}\theta'_c(t)] \cos [2\sqrt{\pi}\theta'_c(0)] \rangle \langle \sin [2\sqrt{\pi}\theta_f(t)] \sin [2\sqrt{\pi}\theta_f(0)] \rangle.
\end{aligned} \tag{19}$$

Evaluation of the bosonic correlation function is standard, see for example Refs. [68, 73]. In terms of the scaling dimension $\Omega = 1 + 1/(1+r)$ of the backscattering operator, the result for the rate is

$$\begin{aligned}
\Gamma(V, T) &= \frac{A^2}{4\hbar^2} \int_{-\infty}^{\infty} dt e^{ieVt/\hbar} \exp \left[-2\Omega \ln \sinh \left(\frac{\pi k_B T |t|}{\hbar} \right) + 2\Omega \ln \frac{\pi k_B T}{\hbar \omega_R} - \Omega i \pi \text{Sign}(t) - 2\Omega \gamma \right] \\
&= \frac{A^2}{4\hbar^2} \frac{\pi}{\Gamma(2\Omega)} \left(\frac{2\pi k_B T}{\hbar \omega_R} \right)^{2\Omega-1} \frac{1}{\omega_R} \exp \left(\frac{eV}{2k_B T} \right) \left| \Gamma \left(\Omega + i \frac{eV}{2\pi k_B T} \right) \right|^2,
\end{aligned} \tag{20}$$

where ω_R is the energy cutoff of the bosonic bath and γ is Euler's constant. Physically, as this rate involves gain of energy, it corresponds to backscattering from the right-moving to left-moving channel [using the convention of Eqs. (3) and (14c)]. The net current is related to the difference of this rate and that in the opposite sense, namely $\Gamma(-V, T)$. Since the energy associated with the bias in each backscattering event is eV , we conclude that the charge carried by each quasi-particle is e . Consequently, the backscattering-related current is $\Delta I(V, T) = e[\Gamma(V, T) - \Gamma(-V, T)]$. Adding this to the perfect transmission when $A = 0$, we arrive at our final result for the I - V curve

$$I(V, T) = \frac{e^2}{h} V \left\{ 1 - \frac{A^2 \pi^2}{\hbar^2 \omega_R^2} \frac{1}{\Gamma(\frac{2}{1+r} + 2)} \left(\frac{2\pi k_B T}{\hbar \omega_R} \right)^{\frac{2}{1+r}} \left| \frac{\Gamma \left(\frac{1}{1+r} + 1 + i \frac{eV}{2\pi k_B T} \right)}{\Gamma \left(1 + i \frac{eV}{2\pi k_B T} \right)} \right|^2 \right\}. \tag{21}$$

This is the main theoretical result of this paper: the nonlinear I - V curve to leading order in the backscattering amplitude A in the critical regime of a strong-coupling QCP (path 1 in Fig. 1). Flow to this QCP occurs by tuning the system (described by the original microscopic Hamiltonian in Sec. II) to be on resonance and to have symmetric source and drain barriers. The flow to the QCP is then cutoff by the temperature or bias. At large bias, a power-law dependence is found, $|dI/dV - e^2/h| \propto V^{2/(1+r)}$, as expected from the equilibrium RG analysis at the end of Sec. IV. A plot of the full result is shown in Fig. 2.

VI. COMPARISON TO EXPERIMENT

Experiments were performed on quantum dots fabricated from carbon nanotubes contacted by Cr/Au electrodes. The electrodes were further connected to the bonding pads by Cr resistors that provided dissipation. For more information on the fabrication and characteristics of the samples, see Refs. [17, 18]. Here we show data from a sample with $r = 0.5$ (for similar data for a sample with $r = 0.75$ see the supplemental material [78]). The value of r is determined in an independent equilibrium measurement of $G(T)$ off resonance, which scales as T^{2r} [17]. Once r is fixed, we check that the equilibrium ($eV \ll k_B T$) value of $1 - G$ on resonance scales

as $T^{2/(1+r)}$, as demonstrated previously [18]. This confirms that the gate voltages controlling the level's energy and the symmetry of the barriers are tuned to their critical values.

For the critical values of the gate voltages, we next consider the conductance in the full range of applied bias—both smaller and larger than $k_B T$, corresponding to the equilibrium and non-equilibrium regimes, respectively. Fig. 2 shows the conductance G , measured in units of e^2/h and rescaled such that at a given temperature $1 - G(V)$ is divided by $1 - G(V=0)$, compared to the full non-linear theoretical result Eq. (21) (solid line). (Note that the value of A in (21) is eliminated in the ratio $[1 - G(V)]/[1 - G(V=0)]$. For other ways of plotting the data, see the supplemental material [78].) Though there are no free parameters in the theory—this is not a fit—the theoretical curve captures the experimental behavior remarkably well.

Comparing closely the experimental and theoretical results, we see two striking features of the theory: first, it captures the *crossover regime* $eV \sim k_B T$ very accurately, and, second, it yields the correct *prefactor* of the universal $\propto V^{2/(1+r)}$ dependence at high bias [83]. Thus our theory goes well beyond the frequently used scaling arguments that produce only the exponent in the scaling regime (the slope on this log-log plot) and not the actual conductance magnitude. *The excellent agreement between the theory and experiment in a wide range of $eV/k_B T$ is a striking confirmation of our far-from-equilibrium calculation.*

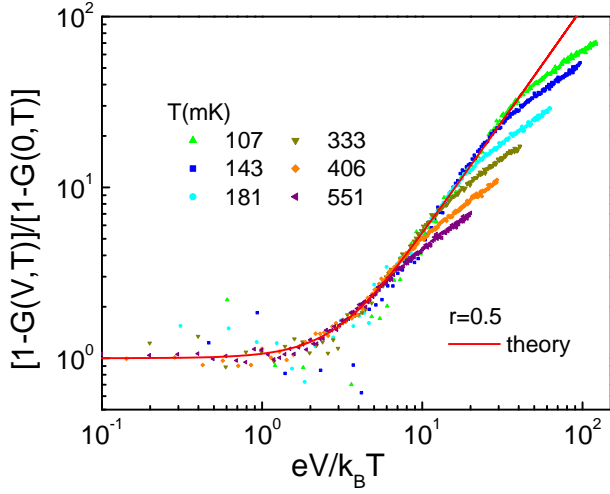


FIG. 2. Conductance measured in the full bias range—from much smaller to much larger than the temperature—presented as the deviation from perfect conductance $1-G(V, T)$ scaled by $1-G(V=0, T)$ and plotted vs. the rescaled bias $eV/k_B T$. Here $G(V, T)$ is the differential conductance $G=(h/e^2) dI/dV$ and $r=0.5$. Gate voltages are tuned to their critical values; thus, for small V and T the system approaches its QCP (see path 1 in Fig. 1). The symbols are the experimental results at the color-coded temperatures. The red line is the result of the non-equilibrium theory [Eq. (21)], in which there are no free parameters. Note the excellent agreement between the theory and data in both the crossover and power-law regimes. At larger V/T , non-universal effects begin to set in due to $1-G(V, T)$ becoming non-negligible compared to 1.

It is important to realize that, unlike measurements that use a weakly coupled electrode as a tunnel probe that measures the equilibrium density of states at finite bias (for example [8, 9, 13, 48, 49]), here the two biased leads remain equally coupled to the quantum dot, creating genuinely nonequilibrium conditions [29, 51].

At high enough $eV/k_B T$, the experimental curves deviate from the theoretical prediction (Fig. 2). There are several possible contributions to this deviation. Because $1-G$ is no longer small, irrelevant operators not included in our effective strong-coupling model [Eq. (15)] may become significant. An additional possible contribution is that the second order analysis of the present model is inadequate at high bias. At the same time, note that the range of applicability of our analytical results is pushed to higher and higher $eV/k_B T$ as the temperature is lowered.

VII. INTERPRETATION AS DYNAMICAL COULOMB BLOCKADE

To enhance the physical understanding of our main results, Eq. (21) and Fig. 2, we rewrite our strong coupling effective system as a fermionic problem and thereby make a direct connection to dynamical Coulomb blockade (DCB) theory. In order to use non-interacting fermions, we choose to refermionize the non-interacting bosonic fields (θ_f, ϕ_c) in Eq. (15), using the bosonization relation Eq. (6) where α now denotes this

pair. It is also convenient to move the bias out of the barrier term by undoing the time-dependent gauge transformation. The coupling term Eq. (15c) is, then, replaced by the two terms

$$\begin{aligned} H_T &= \pi a_0 A \cos [2\sqrt{\pi}\theta'_c(0)] [\psi_L^\dagger(0)\psi_R(0) + \text{h.c.}] \\ H_\mu &= -eV\theta'_c(0)/\sqrt{4\pi}. \end{aligned} \quad (22)$$

The fact that the bias couples to the interacting field θ'_c is a serious complication. However, note that we will calculate the $I-V$ curve only to leading order in A , as in Sec. V. In the expression for the rate, the bias appears only in the energy-conservation δ -function as the particle gains (or loses) energy eV when it backscatters. Note that the excitations of θ'_c and θ_f are tightly linked in the single term in Eq. (15c), leading to a single connection between a given $|i\rangle$ and its $|f\rangle$. Thus, whether the energy eV comes from coupling to the interacting or non-interacting field cannot be distinguished at this order. We can, then, calculate the $I-V$ curve using the bias term

$$H'_\mu = -eV\theta_f(0)/\sqrt{4\pi}. \quad (23)$$

Refermionizing this term using relations analogous to those in Eq. (6), we arrive at the auxiliary model

$$\begin{aligned} H' &= \frac{1}{2} \int_{-\infty}^{\infty} dx [\psi_R^\dagger(x)\partial_x\psi_R(x) - \psi_L^\dagger(x)\partial_x\psi_L(x)] \\ &+ \frac{1}{2} \int_0^\infty dx \left[(1+r)(\partial_x\theta'_c)^2 + \frac{1}{1+r}(\partial_x\phi'_f)^2 \right] \\ &+ \pi a_0 A \cos [2\sqrt{\pi}\theta'_c(0)] \{ \psi_L^\dagger(0)\psi_R(0) + \text{h.c.} \} \\ &+ \frac{eV}{2} \left[\int_{-\infty}^0 dx \psi_R^\dagger(x)\psi_R(x) - \int_0^\infty dx \psi_L^\dagger(x)\psi_L(x) \right]. \end{aligned} \quad (24)$$

Each line of (24) can be interpreted physically: the first line is right- and left- moving non-interacting fermions, second line is an interacting bosonic environment, third line shows that backscattering of the fermions excites the environment, and fourth line accounts for the voltage bias between the right- and left- moving fermions.

We thus recognize the form for tunneling of non-interacting particles through a barrier in the presence of an environment [68–70], albeit with a strange barrier and strange environment. Tunneling through the barrier consists of backscattering between two chiral fermion modes, and the environment θ'_c involves a nonlinear combination of the original electrons and environment [the rotation Eq. (9) applies to quantities in the exponent]. Nevertheless, the standard techniques of DCB theory [68–70] can be applied to obtain the nonlinear $I-V$ curve to second order in A (for details of the calculation see the supplemental material [78]). The result [56, 78, 84] is the same as in the last section, Eq. (21), with the coefficient of the correction $(A\pi/\hbar\omega_R)^2$ replaced by $(h/e^2)/R_T$, where R_T is the tunneling resistance of the effective barrier in the absence of dissipation.

The equivalence of these two coefficients is shown by considering the standard single-barrier tunneling Hamiltonian. Denote the backscattering amplitude of the fermions by $t_{k,q}$,

where k and q label the initial and final fermionic particle states, $H_T = \sum_{k,q} t_{k,q} c_{L,k}^\dagger c_{R,q} + \text{h.c.}$. The standard result for the conductance of a tunneling barrier when the amplitude is momentum independent is $1/R_T = (e^2/h)|\bar{t}|^2[\Xi N(0)]^2$, where $\Xi N(0)$ is the number of states per unit energy and \bar{t} is the average matrix element. In our case, the number of states is the size of the system L divided by the bosonization cutoff a_0 , and the maximum energy for a particle excitation is $\hbar\omega_R$, the cutoff for the bosonic modes ($-\hbar\omega_R$ for a hole excitation). The amplitude \bar{t} follows from Eq. (24) noting that a factor of $1/L$ is introduced in the conversion from continuous x to discrete k . Putting these elements together one finds

$$\frac{1}{R_T} = \frac{e^2}{h} \left(\frac{\pi a_0 A}{L} \right)^2 \left(\frac{L/a_0}{\hbar\omega_R} \right)^2 = \frac{e^2}{h} \left(\frac{\pi A}{\hbar\omega_R} \right)^2. \quad (25)$$

Thus the I - V curve that results from a DCB theory treatment of the auxiliary strong-coupling model (24) and that found from the true effective bosonic description (15) are identical.

This allows then the physically intuitive interpretation of the I - V curve Eq. (21) as tunneling of non-interacting fermions (between left-movers and right-movers) in the presence of an environment.

VIII. CONCLUSIONS

We have carried out an analytic calculation of a far-from-equilibrium I - V curve for a system whose control parameters are tuned to a strong-coupling QCP (path 1 in Fig. 1), and then presented experimental results enabling a detailed theory-experiment comparison. The calculation is made possible through an effective bosonic description at strong-coupling. The agreement with the experimental results throughout the crossover and asymptotic regimes, as shown in Fig. 2, is excellent.

A simple physical interpretation is possible because only one of the charge modes in the system couples to the resistive environment, leaving the mode corresponding to fluctuations of the total charge in the dot free. This feature is not present, for instance, in the related problem of resonant tunneling in a Luttinger liquid. It allows us to find the I - V curve, alternatively, from the problem of tunneling between left- and right-moving non-interacting fermions in the presence of a modified environment. The solution to that problem from dynamical Coulomb blockade theory yields an explicit expression for the nonlinear I - V curve. Comparing the results of the bosonic and fermionic calculations, one finds that they are identical.

To our knowledge, this is the first calculation or measurement of a nonequilibrium I - V curve of a system tuned to the critical value of the control parameter. As mentioned in the introduction, our situation is different from the measurements in which a weakly coupled contact measures the equilibrium density of states at finite bias (for example [8, 9, 13, 48, 49]). Here the two biased leads remain equally coupled to the quantum dot, creating genuinely nonequilibrium conditions [29, 51].

A remarkable aspect of this system is that it is fully accessible to both theory and experiment, allowing for a detailed

comparison between the two. This accessibility is characteristic of other nanoscale systems exhibiting boundary QPT as well, see e.g. [9–11], one of the reasons for increasing interest in this topic. As nonequilibrium results in quantum critical states are exceedingly rare, our results provide a valuable bench mark and test case for future studies of nonequilibrium steady states.

ACKNOWLEDGMENTS

We thank E. Novais for helpful discussions. The work in Taiwan (CHC and CYL) was supported by the NSC grants No.98-2918-I-009-06 and No.98-2112-M-009-010-MY3, the MOE-ATU program, and the NCTS of Taiwan, R.O.C. The work in the U.S.A. was supported by the U.S. DOE Office of Science, Division of Materials Sciences and Engineering, under Grants Nos. DE-SC0005237 (GZ and HUB, theory), DE-SC0002765 (CTK, HM, and GF, experiment), and DE-FG02-02ER15354 (AIS, experiment).

Appendix A: Integrating out the Dissipation at Strong Coupling

In this appendix we briefly show the final step in arriving at the effective strong coupling model Eq. (15) by integrating out the environment. We begin by rewriting the free lead and environment Hamiltonian, Eqs. (11a) and (5), in the form of an action,

$$\begin{aligned} S_0 &= S_{\text{Leads}} + S_{\text{Env}} \\ &= \frac{1}{2} \iint d\tau dx [(\partial_x \theta_c)^2 + (\partial_\tau \theta_c)^2 + (\partial_x \theta_f)^2 + (\partial_\tau \theta_f)^2] \\ &\quad + \frac{1}{2} \iint d\tau dx 2r [(\partial_x \vartheta)^2 + (\partial_\tau \vartheta)^2]. \end{aligned} \quad (A1)$$

(We write the action in terms of the θ fields rather than the ϕ because of the boundary conditions connected to the very weak barrier.) Since the action is quadratic except for the backscattering occurring at the origin, the $x \neq 0$ degrees of freedom can be integrated out. If the backscattering is not too strong, the free action is minimized when $\theta(x, \omega_n) = \theta(x=0, \omega_n) \exp(-|\omega_n x|)$ and $\vartheta(x, \omega_n) = \vartheta(x=0, \omega_n) \exp(-|\omega_n x|)$, where ω_n is the Matsubara frequency [59]. We can thus integrate out the $x \neq 0$ part of the system so that the free action becomes zero-dimensional,

$$S_0 = \frac{1}{\beta} \sum_{\omega_n} |\omega_n| [\theta_f(\omega_n)^2 + \theta_c(\omega_n)^2 + 2r\vartheta(\omega_n)^2], \quad (A2)$$

where all the fields are evaluated at $x = 0$.

The coupling between the leads and the environment is given by the second term in Eq. (14c), which in action form is

$$\begin{aligned} S_{\text{coup.}} &= -i2\sqrt{2} \int d\tau r [\partial_x \vartheta(0)] \theta_c(0) \\ &= i \frac{2\sqrt{2}r}{\beta} \sum_{\omega_n} |\omega_n| \vartheta(\omega_n) \theta_c(-\omega_n), \end{aligned} \quad (A3)$$

rewritten in Matsubara summation form. Since this term is a quadratic product of ϑ and θ_c , we can easily integrate out the environment ϑ with a Gaussian path integral. The integral is done with the partition function,

$$Z = \iiint D[\theta_c]D[\theta_f]D[\vartheta]e^{-S_0[\theta_c, \theta_f, \vartheta] - S_{\text{coup.}}[\theta_c, \vartheta] - S_{\text{T}}[\theta_c, \theta_f]}, \quad (\text{A4})$$

after which the effective partition function becomes

$$Z^{\text{eff}} = \iint D[\theta_c]D[\theta_f]e^{-S'_{\text{Leads}} - S_{\text{T}}}, \quad (\text{A5})$$

where

$$S'_{\text{Leads}} = \frac{1}{2} \iint d\tau dx [(\partial_x \theta_f)^2 + (\partial_\tau \theta_f)^2 + (1+r)(\partial_x \theta_c)^2 + (1+r)(\partial_\tau \theta_c)^2]. \quad (\text{A6})$$

Here we have extended the fields back to their original semi-infinite domains. Notice that the interaction between dissipative environment and the θ_c field has been effectively incorporated into the free action of θ_c so that it becomes effectively interacting with strength $1/(1+r)$. Finally, we convert to the Hamiltonian form and, to be consistent with the notation

of the main text, relabel (θ_c, ϕ_f) as (θ'_c, ϕ'_f) . The relabeling should also be carried out, of course, in the backscattering term, Eq. (13), $H_{\text{T}} \rightarrow A \cos(2\sqrt{\pi}\theta'_c + eVt) \sin(2\sqrt{\pi}\theta'_f)$. We thus arrive at Eq. (15).

Appendix B: Connection to backscattering operator in LL

The form of the backscattering term in H^{eff} , Eq. (15), is convenient for the calculation of the I - V curve in the Sec. V. In this appendix, we show that it is also consistent with the form of the backscattering operator in resonant tunneling through a LL at zero bias [60], namely $\cos[2\sqrt{\pi}\theta'(0)]\partial_x\theta'(0)$, where $\theta'(x)$ is the interacting field describing the LL. Note in this regard that both the c and f modes are interacting in a LL and related to $\theta'(x)$. To arrive at this form from Eq. (15c), expand about the midpoint of the two barriers and call this point $x=0$. Then from Eq. (12), $\theta'_c \approx \theta'(0)$ and $\theta'_f \approx \partial_x\theta'(0)\ell/2$. Since $\partial_x\theta'(0)\ell/2$ is small and fluctuating, the $\sin[2\sqrt{\pi}\theta'_f(0)]$ factor is simply expanded to yield $\pi^{3/2}\partial_x\theta'(0)/2k_F$, where we have used $k_F\ell = \pi/2$ on resonance. Combining this with $\cos\theta'_c \approx \cos\theta'(0)$, we arrive at the expression above for backscattering from two barriers in a LL.

-
- [1] Lincoln D. Carr, *Understanding Quantum Phase Transitions* (CRC Press, Boca Raton, Florida, 2011).
- [2] Subir Sachdev, *Quantum Phase Transitions*, 2nd ed. (Cambridge University Press, Cambridge, 2011).
- [3] M. Vojta, “Impurity quantum phase transitions,” *Philos. Mag.* **86**, 1807–1846 (2006).
- [4] L. Amico, R. Fazio, A. Osterloh, and V. Vedral, “Entanglement in many-body systems,” *Rev. Mod. Phys.* **80**, 517–576 (2008).
- [5] A. Polkovnikov, K. Sengupta, A. Silva, and M. Vengalattore, “Colloquium: Nonequilibrium dynamics of closed interacting quantum systems,” *Rev. Mod. Phys.* **83**, 863–883 (2011).
- [6] H. Aoki, N. Tsuji, M. Eckstein, M. Kollar, T. Oka, and P. Werner, “Nonequilibrium dynamical mean-field theory and its applications,” *Rev. Mod. Phys.* **86**, 779–837 (2014).
- [7] J. Eisert, M. Friesdorf, and C. Gogolin, “Quantum many-body systems out of equilibrium,” *Nat. Phys.* **11**, 124–130 (2015).
- [8] R. M. Potok, I. G. Rau, H. Shtrikman, Y. Oreg, and D. Goldhaber-Gordon, “Observation of the two-channel Kondo effect,” *Nature* **446**, 167–171 (2007).
- [9] A. J. Keller, L. Peeters, C. P. Moca, I. Weymann, D. Mahalu, V. Umansky, G. Zarand, and D. Goldhaber-Gordon, “Universal Fermi liquid crossover and quantum criticality in a mesoscopic system,” *Nature* **526**, 237–240 (2015).
- [10] Z. Iftikhar, S. Jezouin, A. Anthore, U. Gennser, F. D. Parmentier, A. Cavanna, and F. Pierre, “Two-channel kondo effect and renormalization flow with macroscopic quantum charge states,” *Nature* **526**, 233–236 (2015).
- [11] Z. Iftikhar, A. Anthore, A. K. Mitchell, F. D. Parmentier, U. Gennser, A. Ouerghi, A. Cavanna, C. Mora, P. Simon, and F. Pierre, “Tunable quantum criticality and super-ballistic transport in a “charge” Kondo circuit,” *Science*, eaan5592 (2018).
- [12] R. Maurand, T. Meng, E. Bonet, S. Florens, L. Marty, and W. Wernsdorfer, “First-order $0-\pi$ quantum phase transition in the Kondo regime of a superconducting carbon-nanotube quantum dot,” *Phys. Rev. X* **2**, 011009 (2012).
- [13] W. Chang, V. E. Manucharyan, T. S. Jespersen, J. Nyård, and C. M. Marcus, “Tunneling spectroscopy of quasiparticle bound states in a spinful Josephson junction,” *Phys. Rev. Lett.* **110**, 217005 (2013).
- [14] R. Delagrè, R. Weil, A. Kasumov, M. Ferrier, H. Bouchiat, and R. Deblock, “ $0-\pi$ quantum transition in a carbon nanotube Josephson junction: Universal phase dependence and orbital degeneracy,” *Phys. Rev. B* **93**, 195437 (2016).
- [15] R. Härtle, G. Cohen, D. R. Reichman, and A. J. Millis, “Transport through an Anderson impurity: Current ringing, nonlinear magnetization, and a direct comparison of continuous-time quantum Monte Carlo and hierarchical quantum master equations,” *Phys. Rev. B* **92**, 085430 (2015).
- [16] Yu. Bomze, H. Mebrahtu, I. Borzenets, A. Makarovski, and G. Finkelstein, “Resonant tunneling in a dissipative environment,” *Phys. Rev. B* **79**, 241402 (2009).
- [17] H. T. Mebrahtu, I. V. Borzenets, Dong E. Liu, Huaixiu Zheng, Yu. V. Bomze, A. I. Smirnov, H. U. Baranger, and G. Finkelstein, “Quantum phase transition in a resonant level coupled to interacting leads,” *Nature* **488**, 61–64 (2012).
- [18] H. T. Mebrahtu, I. V. Borzenets, H. Zheng, Yu. V. Bomze, A. I. Smirnov, S. Florens, H. U. Baranger, and G. Finkelstein, “Observation of Majorana quantum critical behavior in a resonant level coupled to a dissipative environment,” *Nat. Phys.* **9**, 732–737 (2013), arXiv:1212.3857.
- [19] A. M. Chang, “Chiral Luttinger liquids at the fractional quantum Hall edge,” *Rev. Mod. Phys.* **75**, 1449–1505 (2003).
- [20] M. Grobis, I. G. Rau, R. M. Potok, and D. Goldhaber-Gordon, “Kondo effect in mesoscopic quantum dots,” in *Handbook of Magnetism and Advanced Magnetic Materials*, Vol. 5, edited by H. Kronmüller and S. Parkin (Wiley, New York, 2007) pp. 2703–

- 2724, and arXiv:cond-mat/0611480.
- [21] A. M. Chang and J. C. Chen, “The Kondo effect in coupled-quantum dots,” *Rep. Prog. Phys.* **72**, 096501 (2009).
- [22] A. P. Micolich, “What lurks below the last plateau: Experimental studies of the 0.7 conductance anomaly in one-dimensional systems,” *J. Phys. Cond. Matt.* **23**, 443201 (2011).
- [23] A. Martín-Rodero and A. Levy-Yeyati, “Josephson and Andreev transport through quantum dots,” *Adv. Phys.* **60**, 899–958 (2011).
- [24] I. G. Rau, S. Amasha, Y. Oreg, and D. Goldhaber-Gordon, “Quantum phase transitions in quantum dots,” in *Understanding Quantum Phase Transitions*, edited by L. D. Carr (CRC Press, Boca Raton, 2011) pp. 341–367.
- [25] A. V. Kretinin, H. Shtrikman, D. Goldhaber-Gordon, M. Hanl, A. Weichselbaum, J. von Delft, T. Costi, and D. Mahalu, “Spin- $\frac{1}{2}$ kondo effect in an inas nanowire quantum dot: Unitary limit, conductance scaling, and zeeman splitting,” *Phys. Rev. B* **84**, 245316 (2011).
- [26] S. Jezouin, M. Albert, F. D. Parmentier, A. Anthore, U. Gennser, A. Cavanna, I. Safi, and F. Pierre, “Tomonaga-Luttinger physics in electronic quantum circuits,” *Nat. Commun.* **4**, 1802 (2013).
- [27] M. Ferrier, T. Arakawa, T. Hata, R. Fujiwara, R. Delagrangé, R. Weil, R. Deblock, R. Sakano, A. Oguri, and K. Kobayashi, “Universality of non-equilibrium fluctuations in strongly correlated quantum liquids,” *Nat. Phys.* **12**, 230–235 (2016).
- [28] A. Anthore, Z. Iftikhar, E. Boulat, F. D. Parmentier, A. Cavanna, A. Ouerghi, U. Gennser, and F. Pierre, “Circuit quantum simulation of a Tomonaga-Luttinger liquid with an impurity,” arXiv:1809.02017 (2018).
- [29] Y. Meir and N. S. Wingreen, “Landauer formula for the current through an interacting electron region,” *Phys. Rev. Lett.* **68**, 2512–2515 (1992).
- [30] P. Fendley, A. W. W. Ludwig, and H. Saleur, “Exact nonequilibrium transport through point contacts in quantum wires and fractional quantum Hall devices,” *Phys. Rev. B* **52**, 8934–8950 (1995).
- [31] A. Schiller and S. Hershfield, “Toulouse limit for the nonequilibrium Kondo impurity: Currents, noise spectra, and magnetic properties,” *Phys. Rev. B* **58**, 14978 (1998); K. Majumdar, A. Schiller, and S. Hershfield, “Nonequilibrium Kondo impurity: Perturbation about an exactly solvable point,” *Phys. Rev. B* **57**, 2991–2999 (1998).
- [32] A. Rosch, J. Paaske, J. Kroha, and P. Wölfle, “Nonequilibrium transport through a Kondo dot in a magnetic field: Perturbation theory and poor man’s scaling,” *Phys. Rev. Lett.* **90**, 076804 (2003).
- [33] F. Heidrich-Meisner, A. E. Feiguin, and E. Dagotto, “Real-time simulations of nonequilibrium transport in the single-impurity Anderson model,” *Phys. Rev. B* **79**, 235336 (2009).
- [34] C.-H. Chung, K. Le Hur, M. Vojta, and P. Wölfle, “Nonequilibrium transport at a dissipative quantum phase transition,” *Phys. Rev. Lett.* **102**, 216803 (2009); C.-H. Chung, K. Le Hur, G. Finkelstein, M. Vojta, and P. Wölfle, “Nonequilibrium quantum transport through a dissipative resonant level,” *Phys. Rev. B* **87**, 245310 (2013).
- [35] I. Safi and P. Joyez, “Time-dependent theory of nonlinear response and current fluctuations,” *Phys. Rev. B* **84**, 205129 (2011).
- [36] V. Koerting, B. M. Andersen, K. Flensberg, and J. Paaske, “Nonequilibrium transport via spin-induced subgap states in superconductor/quantum dot/normal metal cotunnel junctions,” *Phys. Rev. B* **82**, 245108 (2010).
- [37] M. Pletyukhov and H. Schoeller, “Nonequilibrium Kondo model: Crossover from weak to strong coupling,” *Phys. Rev. Lett.* **108**, 260601 (2012).
- [38] G. Cohen, E. Gull, D. R. Reichman, and A. J. Millis, “Green’s Functions from Real-Time Bold-Line Monte Carlo Calculations: Spectral Properties of the Nonequilibrium Anderson Impurity Model,” *Phys. Rev. Lett.* **112**, 146802 (2014).
- [39] R. Härtle and A. J. Millis, “Formation of nonequilibrium steady states in interacting double quantum dots: When coherences dominate the charge distribution,” *Phys. Rev. B* **90**, 245426 (2014).
- [40] A. Dorda, M. Ganahl, H. G. Evertz, W. von der Linden, and E. Arrighi, “Auxiliary master equation approach within matrix product states: Spectral properties of the nonequilibrium Anderson impurity model,” *Phys. Rev. B* **92**, 125145 (2015).
- [41] C. Altimiras, F. Portier, and P. Joyez, “Interacting electro-dynamics of short coherent conductors in quantum circuits,” *Phys. Rev. X* **6**, 031002 (2016).
- [42] E. Sela and I. Affleck, “Nonequilibrium transport through double quantum dots: Exact results near a quantum critical point,” *Phys. Rev. Lett.* **102**, 047201 (2009).
- [43] E. Sela and I. Affleck, “Nonequilibrium critical behavior for electron tunneling through quantum dots in an Aharonov-Bohm circuit,” *Phys. Rev. B* **79**, 125110 (2009).
- [44] A. K. Mitchell, L. A. Landau, L. Fritz, and E. Sela, “Universality and scaling in a charge two-channel Kondo device,” *Phys. Rev. Lett.* **116**, 157202 (2016).
- [45] B. Béri, “Exact nonequilibrium transport in the topological Kondo effect,” *Phys. Rev. Lett.* **119**, 027701 (2017).
- [46] L. Aviad Landau, Eyal Cornfeld, and Eran Sela, “Charge fractionalization in the two-channel kondo effect,” *Phys. Rev. Lett.* **120**, 186801 (2018).
- [47] In the final stages of preparing this paper, we became aware of the beautiful work in Ref. [28] studying tunneling through a single barrier in the presence of dissipation. While both fixed points of that problem are thoroughly studied in [28], there is no quantum critical state in that problem and so nothing comparable to properties along path 1 in Fig. 1—all of the results are for a cross-over like path 2.
- [48] R. Leturcq, L. Schmid, K. Ensslin, Y. Meir, D. C. Driscoll, and A. C. Gossard, “Probing the Kondo density of states in a three-terminal quantum ring,” *Phys. Rev. Lett.* **95**, 126603 (2005).
- [49] A. Makarovski, J. Liu, and G. Finkelstein, “Evolution of transport regimes in carbon nanotube quantum dots,” *Phys. Rev. Lett.* **99**, 066801 (2007).
- [50] Thomas Ihn, *Semiconductor Nanostructures* (Oxford University Press, Oxford, 2010), pp. 199, 310-4.
- [51] M. Pustilnik, L. Borda, L. I. Glazman, and J. von Delft, “Quantum phase transition in a two-channel-Kondo quantum dot device,” *Phys. Rev. B* **69**, 115316 (2004).
- [52] M. P. A. Fisher and L. I. Glazman, “Transport in a one-dimensional Luttinger liquid,” in *Mesoscopic Electron Transport*, edited by L. L. Sohn, L. P. Kouwenhoven, and G. Schön (Kluwer, New York, 1997) pp. 331–373.
- [53] I. Affleck, “Quantum impurity problems in condensed matter physics,” in *Exact Methods in Low-dimensional Statistical Physics and Quantum Computing: Lecture Notes of the Les Houches Summer School: Volume 89, July 2008*, edited by J. Jacobsen, S. Ouvry, V. Pasquier, D. Serban, and L. Cugliandolo (Oxford Univ. Press, 2010) pp. 3–64.
- [54] K. A. Matveev and L. I. Glazman, “Coulomb blockade of tunneling into a quasi-one-dimensional wire,” *Phys. Rev. Lett.* **70**, 990–993 (1993).

- [55] Karsten Flensberg, “Capacitance and conductance of mesoscopic systems connected by quantum point contacts,” *Phys. Rev. B* **48**, 11156–11166 (1993).
- [56] M. Sasseti and U. Weiss, “Transport of 1d interacting electrons through barriers and effective tunnelling density of states,” *EPL (Europhysics Letters)* **27**, 311 (1994).
- [57] I. Safi and H. Saleur, “One-channel conductor in an Ohmic environment: Mapping to a Tomonaga-Luttinger liquid and full counting statistics,” *Phys. Rev. Lett.* **93**, 126602 (2004).
- [58] K. Le Hur and Mei-Rong Li, “Unification of electromagnetic noise and Luttinger liquid via a quantum dot,” *Phys. Rev. B* **72**, 073305 (2005).
- [59] C. L. Kane and M. P. A. Fisher, “Transmission through barriers and resonant tunneling in an interacting one-dimensional electron gas,” *Phys. Rev. B* **46**, 15233–15262 (1992); “Resonant tunneling in an interacting one-dimensional electron gas,” *Phys. Rev. B* **46**, 7268–7271(R) (1992).
- [60] S. Eggert and I. Affleck, “Magnetic impurities in half-integer-spin Heisenberg antiferromagnetic chains,” *Phys. Rev. B* **46**, 10866–10883 (1992).
- [61] A. Furusaki and N. Nagaosa, “Resonant tunneling in a Luttinger liquid,” *Phys. Rev. B* **47**, 3827–3831 (1993).
- [62] A. Furusaki, “Resonant tunneling through a quantum dot weakly coupled to quantum wires or quantum Hall edge states,” *Phys. Rev. B* **57**, 7141–7148 (1998).
- [63] Yu. V. Nazarov and L. I. Glazman, “Resonant tunneling of interacting electrons in a one-dimensional wire,” *Phys. Rev. Lett.* **91**, 126804 (2003).
- [64] D. G. Polyakov and I. V. Gornyi, “Transport of interacting electrons through a double barrier in quantum wires,” *Phys. Rev. B* **68**, 035421 (2003).
- [65] A. Komnik and A. O. Gogolin, “Resonant tunneling between Luttinger liquids: A solvable case,” *Phys. Rev. Lett.* **90**, 246403 (2003).
- [66] V. Meden, T. Enss, S. Andergassen, W. Metzner, and K. Schönhammer, “Correlation effects on resonant tunneling in one-dimensional quantum wires,” *Phys. Rev. B* **71**, 041302 (2005).
- [67] M. Goldstein and R. Berkovits, “Duality between different geometries of a resonant level in a Luttinger liquid,” *Phys. Rev. Lett.* **104**, 106403 (2010).
- [68] G.-L. Ingold and Yu.V. Nazarov, “Charge tunneling rates in ultrasmall junctions,” in *Single Charge Tunneling: Coulomb Blockade Phenomena in Nanostructures*, edited by H. Grabert and M. H. Devoret (Plenum, New York, 1992) pp. 21–107, and arXiv:cond-mat/0508728.
- [69] Yu. V. Nazarov and Y. M. Blanter, *Quantum Transport: Introduction to Nanoscience* (Cambridge University Press, Cambridge, 2009).
- [70] M. H. Devoret, D. Esteve, and C. Urbina, “Single electron phenomena in metallic nanostructures,” in *Mesoscopic Quantum Physics: Les Houches Session LXI*, edited by E. Akkermans, G. Montambaux, Pichard J.-L., and J. Zinn-Justin (Elsevier, Amsterdam, 1995) pp. 605–658.
- [71] M. H. Devoret, “Quantum fluctuations in electrical circuits,” in *Quantum Fluctuations: Les Houches Session LXIII*, edited by S. Reynaud, E. Giacobino, and J. Zinn-Justin (Elsevier, Amsterdam, 1997) p. 351.
- [72] Dong E. Liu, Huaixiu Zheng, G. Finkelstein, and H. U. Baranger, “Tunable quantum phase transitions in a resonant level coupled to two dissipative baths,” *Phys. Rev. B* **89**, 085116 (2014).
- [73] Thierry Giamarchi, *Quantum Physics in One Dimension* (Oxford University Press, New York, 2004).
- [74] J. Honer and U. Weiss, “Nonlinear conductance and noise in boundary sine-gordon and related models,” *Chemical Physics* **375**, 265 – 275 (2010), in Stochastic processes in Physics and Chemistry (in honor of Peter Hänggi).
- [75] E. Wong and I. Affleck, “Tunneling in quantum wires: A boundary conformal field theory approach,” *Nucl. Phys. B* **417**, 403–438 (1994).
- [76] At the QCP, certain degrees of freedom associated with the dot become decoupled and contribute a boundary entropy. The best known example is the $\ln(\sqrt{2})$ entropy at the Emery-Kivelson point due to the decoupled Majorana fermion. In our case, the boundary entropy can be calculated from conformal field theory to be $\ln(\sqrt{1+r})$ [75, 85].
- [77] The effect of the region $|x| < \ell/2$ of the original wire on the charge transport (backscattering and leads) is included here; typically, there are boundary degrees of freedom that become decoupled at the fixed point [60, 75, 76].
- [78] In the Supplemental Material, we address five topics: (i) the derivation of the RG equation (16), (ii) an approximate RG argument for the I - V curve, (iii) experimental data for another value of r , namely $r = 0.75$, (iv) the plotting of the $r = 0.5$ data on different scales, and (v) the calculation of the final expression for the I - V curve in Eq. (21) using dynamical Coulomb blockade theory.
- [79] To explicitly obtain a translationally invariant system at the QCP, first rescale θ'_c and ϕ'_f in Eq. (15b) so as to absorb the factors of $(1+r)^{\pm 1}$. Since there is no interaction, this can be done without any compensating change in other terms. Then combine the flavor and charge fields into fields defined for all x , e.g. $\theta'(x > 0) = \theta'_c(x) + \theta_f(x)$, $\theta'(x < 0) = \theta'_c(-x) - \theta_f(-x)$, and similarly for $\phi(x)$. The Hamiltonian now becomes $\int_{-\infty}^{\infty} dx [(\partial_x \theta')^2 + (\partial_x \phi')^2]$, which is manifestly translationally invariant.
- [80] Hartmut Haug and A.-P. Jauho, *Quantum Kinetics in Transport and Optics of Semiconductors*, 2nd ed. (Springer-Verlag, Berlin, 2008).
- [81] L. S. Levitov and M. Reznikov, “Counting statistics of tunneling current,” *Phys. Rev. B* **70**, 115305 (2004).
- [82] A. O. Gogolin and A. Komnik, “Towards full counting statistics for the Anderson impurity model,” *Phys. Rev. B* **73**, 195301 (2006).
- [83] The absolute magnitude of the current in the power-law scaling regime is a key prediction of weak-coupling DCB theory. Here, because of the unknown amplitude A in the effective strong-coupling model Eq. (15) or (24), we do not have such a prediction. However, for the normalized quantity plotted, DCB theory does give a definite value of the prefactor because it is fixed by the way the theory transitions from the crossover to the asymptotic regime.
- [84] W. Zheng, J. R. Friedman, D. V. Averin, S. Y. Han, and J. E. Lukens, “Observation of strong Coulomb blockade in resistively isolated tunnel junctions,” *Sol. State Comm.* **108**, 839–843 (1998).
- [85] H. Zheng, S. Florens, and H. U. Baranger, “Transport signatures of Majorana quantum criticality realized by dissipative resonant tunneling,” *Phys. Rev. B* **89**, 235135 (2014).

Supplemental Material for

“Universal Nonequilibrium I - V Curve at an Interacting Impurity Quantum Critical Point”

Gu Zhang, Chung-Hou Chung, Chung-Ting Ke, C.-Y. Lin, Henok Mebrahtu,
Alex I. Smirnov, Gleb Finkelstein, and Harold U. Baranger

(Dated: 23 September 2018)

In this Supplemental Material, we provide details on five topics: (i) in Sec. **S1**, the derivation of the equilibrium RG equation, (16) of the main text, (ii) in **S2**, an approximate RG argument for the I - V curve, (iii) in **S3**, experimental data for another value of r , namely $r = 0.75$, (iv) in **S4**, the plotting of the $r = 0.5$ data on axes other than the log-log shown in Fig. 2 of the main text, and (v) in **S5**, the calculation of the final expression for the I - V curve in Eq. (21) of the main text using dynamical Coulomb blockade theory.

Appendix **S1: Renormalization Group (RG) Equation at Tree Level**

In this section, we provide a detailed derivation of Eq. (16) in the main text using standard methods. Basic techniques in this section come from the text “Condensed Matter Field Theory” Ref. [S1].

We start with the effective Hamiltonian Eq. (15) in the main text with $V = 0$ (i.e. in equilibrium). The first step is to integrate out the degrees of freedom for $x \neq 0$ following the procedure described in Appendix A, as these are quadratic terms in the Hamiltonian. In this way, the problem is rewritten in the form of a zero-dimensional action (all fields are evaluated at $x = 0$),

$$\begin{aligned}
 S^{\text{eff}} &= S_0^{\text{eff}} + S_{\text{T}} \\
 &= \frac{1}{\beta} \sum_{\omega_n} |\omega_n| [|\theta_f(\omega_n)|^2 + (1+r)|\theta'_c(\omega_n)|] + A \int d\tau \cos [2\sqrt{\pi}\theta'_c(\tau)] \sin [2\sqrt{\pi}\theta_f(\tau)] \\
 &= \int_{|\omega| < \Lambda} \frac{d\omega}{2\pi} [|\theta_f(\omega)|^2 |\omega| + (1+r)|\theta'_c(\omega)|^2 |\omega|] + A \int d\tau \cos [2\sqrt{\pi}\theta'_c(\tau)] \sin [2\sqrt{\pi}\theta_f(\tau)],
 \end{aligned} \tag{S1}$$

where Λ is the energy cutoff and the substitution $\sum_{\omega_n} \rightarrow \int \frac{d\omega}{2\pi}$ transforms the free action into an integral form. As usual for RG, we decrease the cutoff from Λ to $\Lambda - d\Lambda$ and divide the field into fast and slow modes denoted by $>$ and $<$, respectively,

$$\begin{aligned}
 \theta(\tau) &= \frac{1}{\beta} \int \frac{d\omega}{2\pi} e^{-i\omega\tau} \theta(\omega) \\
 &= \frac{1}{\beta} \int_{|\omega| < \Lambda - d\Lambda} \frac{d\omega}{2\pi} e^{-i\omega\tau} \theta(\omega) + \frac{1}{\beta} \int_{\Lambda - d\Lambda < |\omega| < \Lambda} \frac{d\omega}{2\pi} e^{-i\omega\tau} \theta(\omega) \\
 &\equiv \theta_{<}(\tau) + \theta_{>}(\tau).
 \end{aligned} \tag{S2}$$

Based on these definitions, the action is divided into three parts: $S_{>}^{\text{eff}} + S_{<}^{\text{eff}} + S_I^{\text{eff}}$ where $>$, $<$, and I represent the fast mode, the slow mode, and the interaction between them, respectively, with

$$\begin{aligned}
 S_{<}^{\text{eff}} &= \int_{|\omega| < \Lambda - d\Lambda} \frac{d\omega}{2\pi} [|\theta_f(\omega)|^2 |\omega| + (1+r)|\theta'_c(\omega)|^2 |\omega|] \\
 S_{>}^{\text{eff}} &= \int_{\Lambda - d\Lambda < |\omega| < \Lambda} \frac{d\omega}{2\pi} [|\theta_f(\omega)|^2 |\omega| + (1+r)|\theta'_c(\omega)|^2 |\omega|] \\
 S_I^{\text{eff}} &= A \int d\tau \cos \{2\sqrt{\pi} [\theta'_{c<}(\tau) + \theta'_{c>}(\tau)]\} \sin \{2\sqrt{\pi} [\theta_{f<}(\tau) + \theta_{f>}(\tau)]\}.
 \end{aligned} \tag{S3}$$

Notice that the $>$ and $<$ parts come from the free quadratic action while the I part comes from the backscattering term.

In the RG process, parameters are effectively “flowing” such that the system’s partition function remains invariant. When we divide the action into fast and slow modes, the partition function becomes

$$\begin{aligned} Z &= \iiint D\theta'_{c<} D\theta_{f<} D\theta'_{c>} D\theta_{f>} e^{-S_{<}^{\text{eff}} - S_{>}^{\text{eff}} - S_I^{\text{eff}}} \\ &= \iint D\theta'_{c<} D\theta_{f<} e^{-S_{<}^{\text{eff}}} \iint D\theta'_{c>} D\theta_{f>} e^{-S_{>}^{\text{eff}}} e^{-S_I^{\text{eff}}} \\ &= \iint D\theta'_{c<} D\theta_{f<} e^{-S_{<}^{\text{eff}}} \langle e^{-S_I^{\text{eff}}} \rangle_{>}, \end{aligned} \quad (\text{S4})$$

where the expectation is calculated over all fast modes. Since the backscattering A is small, we approximate $\langle e^{-S_I^{\text{eff}}} \rangle_{>} \approx e^{-\langle S_I^{\text{eff}} \rangle_{>}}$, which can be calculated as

$$\begin{aligned} \langle S_I^{\text{eff}} \rangle_{>} &= \iint D\theta'_{c>} D\theta_{f>} e^{-S_{>}^{\text{eff}}} A \int d\tau \cos \{2\sqrt{\pi} [\theta'_{c<}(\tau) + \theta'_{c>}(\tau)]\} \sin \{2\sqrt{\pi} [\theta_{f<}(\tau) + \theta_{f>}(\tau)]\} \\ &= \frac{A}{4i} \sum_{\gamma, \eta = \pm 1} \int d\tau \eta e^{i2\sqrt{\pi}[\gamma\theta'_{c<} + \eta\theta_{f<}]} \int D\theta'_c e^{-S_{c>}^{\text{eff}}} e^{i2\sqrt{\pi}\gamma \int_{>} \frac{d\omega}{2\pi} \theta'_c(\omega)} \int D\theta_f e^{-S_{f>}^{\text{eff}}} e^{i2\sqrt{\pi}\eta \int_{>} \frac{d\omega}{2\pi} \theta_f(\omega)}, \end{aligned} \quad (\text{S5})$$

where $S_{c>}^{\text{eff}} = \int_{\Lambda-d\Lambda < |\omega| < \Lambda} \frac{d\omega}{2\pi} [(1+r)|\theta'_c(\omega)|^2 |\omega|]$ and $S_{f>}^{\text{eff}} = \int_{\Lambda-d\Lambda < |\omega| < \Lambda} \frac{d\omega}{2\pi} [|\theta_f(\omega)|^2 |\omega|]$ are the fast-mode actions. These two integrals are standard Gaussian integrals, whence

$$\begin{aligned} \langle S_I^{\text{eff}} \rangle_{>} &= \frac{A}{4i} \sum_{\gamma, \eta = \pm 1} \int d\tau \eta e^{i2\sqrt{\pi}[\gamma\theta'_{c<} + \eta\theta_{f<}]} e^{-2\pi(1+\frac{1}{1+r}) \int_{\Lambda-d\Lambda}^{\Lambda} d\omega/2\pi |\omega|} \\ &= A e^{-(1+\frac{1}{1+r}) \frac{d\Lambda}{\Lambda}} \int d\tau \cos [2\sqrt{\pi}\theta'_c(\tau)] \sin [2\sqrt{\pi}\theta_f(\tau)]. \end{aligned} \quad (\text{S6})$$

Before we compare Eq. (S6) with the tunneling term in Eq. (S1) at the beginning of this section, we need to rescale the frequency as $\omega = \omega' \Lambda / (\Lambda + d\Lambda)$ such that the cutoff of ω' scales back to Λ . Consequently, to keep the partition function invariant, we have an effective backscattering strength A^{eff} which is related to the original A by

$$A^{\text{eff}} = A + dA = A e^{\frac{d\Lambda}{\Lambda} - (1+\frac{1}{1+r}) \frac{d\Lambda}{\Lambda}} \approx A - A \frac{1}{1+r} \frac{d\Lambda}{\Lambda}. \quad (\text{S7})$$

Now we choose the bandwidth D as the cutoff such that $dD = -d\Lambda$, and we arrive at

$$\frac{dA}{d \ln D} = \frac{1}{1+r} A, \quad (\text{S8})$$

which is Eq. (16) in the main text.

Appendix S2: Approximate RG argument for I - V curve

It is interesting to compare the data and full theoretical results to a much simpler but approximate treatment of the I - V curve that can be developed starting from the equilibrium RG equation, Eq. (S8). Note that A is thus energy dependent, $A(\epsilon) = A_0 \epsilon^{1/(1+r)}$ where A_0 is a constant. This power-law scaling is cut off below T , making A temperature dependent as well, $A(\epsilon, T)$. The differential conductance $G(V, T) = dI/dV$ can be obtained approximately by integrating the spectral function of the transmission

probability $T(\epsilon, T) = 1 - R(\epsilon, T)$ over ϵ with $R \propto A^2$. A more accurate but technically much more complex RG treatment would involve computing $R(\epsilon, T, V)$ out of equilibrium at a finite bias V . This has been done for the single-channel Kondo model [S2, S3] and for a resonant level with gate dissipation [S4], for instance, but not for the more complex two-channel Kondo model that we are dealing with here.

With the approximation $R(\epsilon, T, V) \approx R(\epsilon, T, V=0)$, the non-linear current therefore reads,

$$I(V, T) \approx \frac{e}{h} \int_{-D_0}^{D_0} d\epsilon [1 - R(\epsilon, T)] [f_R(\epsilon) - f_L(\epsilon)], \quad (\text{S9})$$

where $f_{L/R}(\epsilon)$ is the Fermi-Dirac distribution. The normalized reflection probability $R(V, T)/R(0, T)$ from (S9) exhibits a crossover from power-law behavior in V/T ,

$$R(V, T)/R(0, T) \approx (V/T)^{2/(1+r)} \quad \text{for } V/T > 1, \quad (\text{S10})$$

to the constant value 1 for $V/T \rightarrow 0$, as expected from general considerations.

The result of solving Eq. (S9) is plotted in Figs. S1 and S2 (black line) and compared to the full theory of the main text [Eq. (21)] as well as experimental data presented in the next sections. While the power-law behavior is captured by this approximation, the magnitude of the conductance (i.e. the prefactor) and the cross-over from weak to strong bias are not. The explicit bias dependence of the reflection probability $R(\epsilon, T, V)$ [S2, S3] clearly would be essential in moving the RG curve toward the experimental data and the full theory.

Appendix S3: Experimental Data for $r = 0.75$

To confirm the experimental features highlighted in the main text, we present data for $r = 0.75$ in Fig. S1. The agreement between the full theory (red line) and the experiment is excellent. Note in particular that

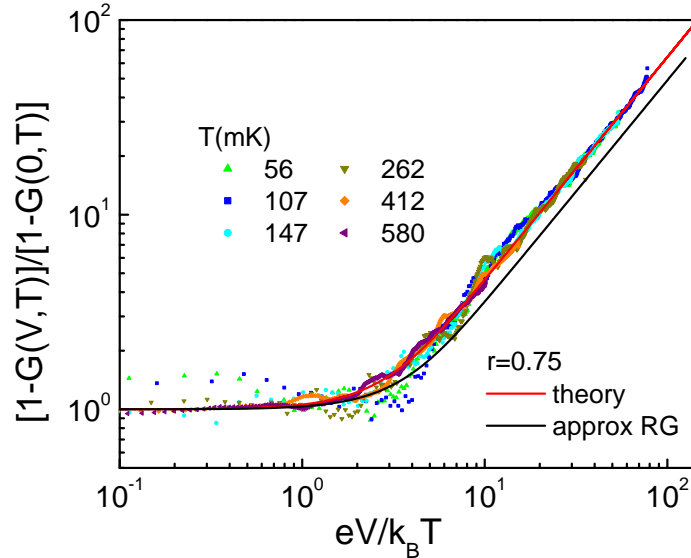


FIG. S1. Deviation from perfect conductance $1 - G(V, T)$, scaled by $1 - G(V = 0, T)$, as a function of $eV/k_B T$ for $r = 0.75$. [$G(V, T)$ is the differential conductance, $G \equiv (h/e^2) dI/dV$.] The symbols are experimental results at the color-coded temperatures. The red and black lines result from the full non-equilibrium and approximate RG theories, respectively, in which there are no free parameters [Eqs. (21) and (S9), respectively]. As for the $r = 0.5$ data shown in the main text, note the excellent agreement between the full theory and the data in both the crossover and power-law regimes. The deviations from scaling seen at high bias in Fig. 2 of the main text were not investigated in this sample (the bias range was limited). The data are taken from Ref. [S5].

the theory goes right through the data in both the crossover region from low to high bias and the scaling regime. Thus our theory goes well beyond the frequently used scaling arguments that produce only the exponent in the scaling regime (the slope on this log-log plot) and not the actual conductance magnitude.

Appendix S4: Experimental Data Other Than log-log Plots

To supplement the comparison between experimental data and the theoretical results, here we provide plots of the same data as in the main text using different combinations of log and linear scales. For the $r = 0.5$ case, in Fig. S2 we plot in four different ways the deviation of the differential conductance from perfect e^2/h : $[1 - G(V, T)]/[1 - G(0, T)]$ vs. $eV/k_B T$ is plotted on (a) log-log, (b) semi-log, (c) linear-log, and (d) linear-linear scales. Focusing on the crossover regime, note the excellent agreement between the experimental data and theoretical results (red line).

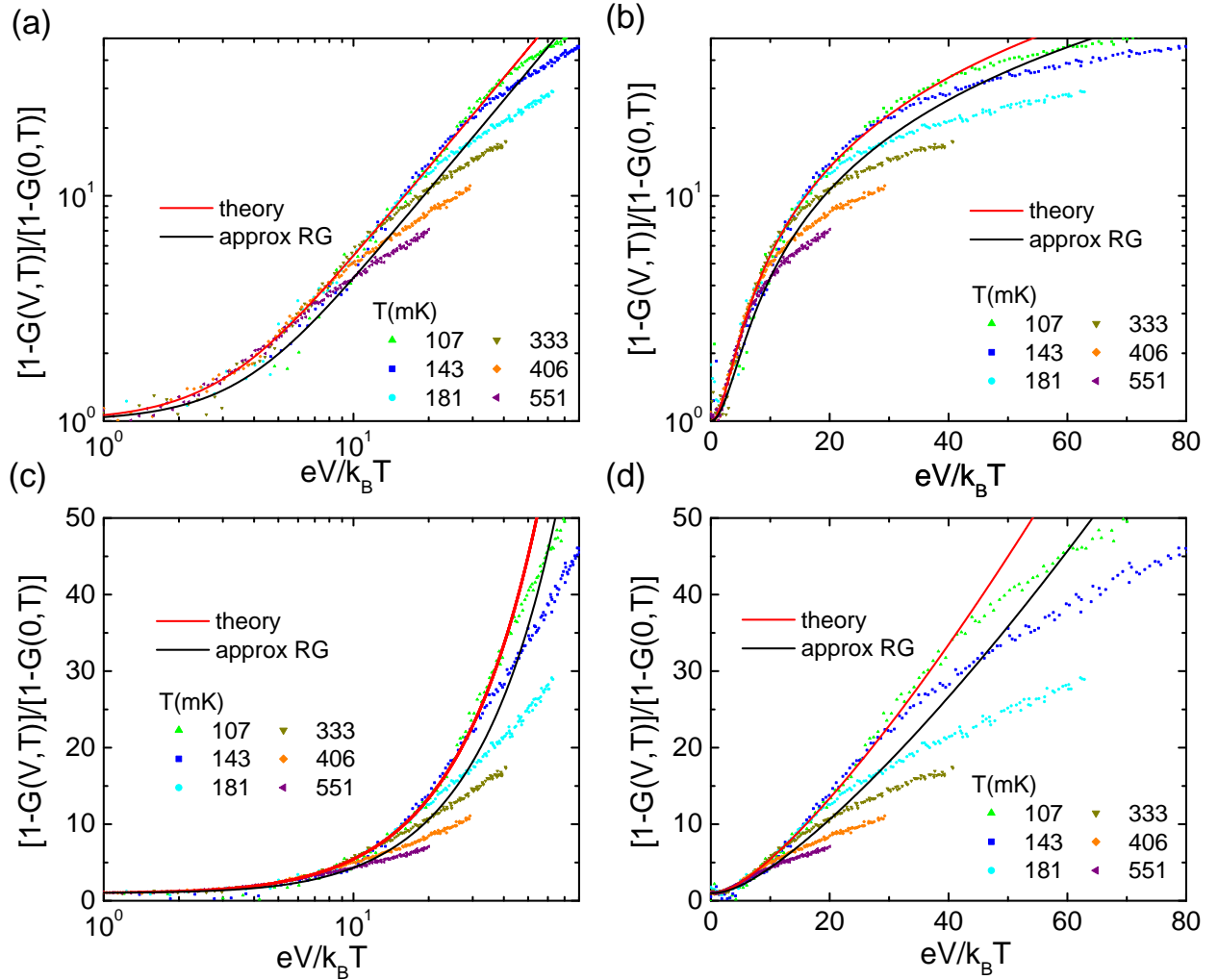


FIG. S2. Comparison between the experimental data and theoretical calculations with dissipation $r = 0.5$ [same data as in in Fig. 2 of main text]. We emphasize the excellent agreement of the theoretical curve (red line) with the experimental data in the crossover regime.

Appendix S5: Derivation of Dynamical Coulomb Blockade (DCB) Result

In this section we derive our result for the I - V curve, main text Eq. (21), from DCB theory, following the classic DCB literature such as [S6–S9]. We start with the refermionized Hamiltonian (24) of the main text,

$$\begin{aligned}
H' &= H_0 + H_r + H_{bias} \\
&= \frac{1}{2} \int_{-\infty}^{\infty} dx \left[\psi_R^\dagger(x) \partial_x \psi_R(x) - \psi_L^\dagger(x) \partial_x \psi_L(x) \right] + \pi a_0 A \cos [2\sqrt{\pi} \theta'_c(0)] \left[\psi_L^\dagger(0) \psi_R(0) + \text{h.c.} \right] \\
&+ \frac{eV}{2} \left[\int_{-\infty}^0 dx \psi_R^\dagger(x) \psi_R(x) - \int_0^{\infty} dx \psi_L^\dagger(x) \psi_L(x) \right] + \frac{1}{2} \int_0^{\infty} dx \left[(1+r)(\partial_x \theta'_c)^2 + \frac{1}{1+r} (\partial_x \phi'_f)^2 \right],
\end{aligned} \tag{S11}$$

which describes two channels of chiral fermions and the environment-coupled tunneling between them. The backscattering Hamiltonian can be rewritten as a product of the bosonic and fermionic parts $H_r = H_r^B H_r^F$, with $H_r^B = \cos [2\sqrt{\pi} \theta'_c(0)]$. Using $|i\rangle$ and $|f\rangle$ to represent the initial and final states, we calculate the rate of backscattering between those two states with Fermi's golden rule $\Gamma_{i \rightarrow f} = \frac{2\pi}{\hbar} |\langle f | H_r | i \rangle|^2 \delta(E_i - E_f)$. The sum over possible initial and final states needed to obtain a macroscopic observable then yields

$$\begin{aligned}
\Gamma(V, T) &= \frac{2\pi}{\hbar} \int_{-\infty}^{+\infty} dE^i dE^f \sum_{R_1^i R_1^f} |\langle E^i | H_r^F | E^f \rangle|^2 |\langle R^i | H_r^B | R^f \rangle|^2 \\
&\times P_\beta(R^i) P_\beta(E) \delta(E^i + E_R^i + eV - E^f - E_R^f),
\end{aligned} \tag{S12}$$

where $|E^i\rangle$ represents the initial state of a quasi-particle in the right-moving channel with energy E^i and $|E^f\rangle$ refers to the left-moving final state. As mentioned in the main text, θ'_c now functions as the dissipative bath, whose initial and final states are given by $|R^{i,f}\rangle$. Meanwhile, the initial density matrix element of bosonic states is described by $P_\beta(R^i) = \langle R^i | \rho_\beta | R^i \rangle$ (here β is a reminder that the density of states is thermally dependent). The fermionic statistics is described by $P_\beta(E)$ [see Eq. (S16) below].

For later convenience, we rewrite the delta function in its integral form

$$\delta(E^i + E_R^i + eV - E^f - E_R^f) = \frac{1}{2\pi\hbar} \int_{-\infty}^{\infty} dt \exp \left[\frac{i}{\hbar} (E^i + E_R^i + eV - E^f - E_R^f) t \right]. \tag{S13}$$

Combining the energy phase of the baths ($E_R^{i,f}$) with the corresponding matrix elements yields

$$\begin{aligned}
&\sum_{R^i, R^f} |\langle R^f | \cos [2\sqrt{\pi} \theta'_c(0)] | R^i \rangle|^2 \cdot e^{\frac{i}{\hbar} (E_R^i - E_R^f) t} P_\beta(R^i) \\
&= \sum_{R^i, R^f} \langle R^i | \cos [2\sqrt{\pi} \theta'_c(t, 0)] | R^f \rangle \langle R^f | \cos [2\sqrt{\pi} \theta'_c(0, 0)] | R^i \rangle P_\beta(R^i) \\
&= \langle \cos [2\sqrt{\pi} \theta'_c(t, 0)] \cos [2\sqrt{\pi} \theta'_c(0, 0)] \rangle = \frac{1}{4} \left\langle e^{i2\sqrt{\pi} \theta'_c(t, 0)} e^{-i2\sqrt{\pi} \theta'_c(0, 0)} \right\rangle = \frac{1}{4} e^{J(t)},
\end{aligned} \tag{S14}$$

where $J(t) \equiv 4\pi \langle [\theta'_c(t) - \theta'_c(0)] \theta'_c(0) \rangle$ is the phase-phase correlation function. [In obtaining (S14), we used the relations [S6] $\langle e^{i\theta(t)} e^{i\theta(0)} \rangle = 0$ and $\langle e^{i2\sqrt{\pi}\alpha\theta(t)} e^{-i2\sqrt{\pi}\alpha\theta(0)} \rangle = e^{\alpha^2 4\pi \langle [\theta(t) - \theta(0)] \theta(0) \rangle} = e^{\alpha^2 J(t)}$.] Since the free bosonic action is quadratic, we can calculate this correlation with a Gaussian integral [S6, S8]

$$J(t) = -\frac{2}{1+r} \ln \sinh \left(\frac{\pi k_B T |t|}{\hbar} \right) + \frac{2}{1+r} \ln \frac{\pi k_B T}{\hbar \omega_R} - \frac{2}{1+r} \frac{i\pi}{2} \text{Sign}(t) - \frac{2}{1+r} \gamma, \tag{S15}$$

where ω_R is the energy cutoff of the bosonic bath and γ is Euler's constant.

Next we deal with the fermionic part. In the DCB method [S6], the backscattering barrier is treated as an effective backscattering resistance R_T so that the fermionic matrix element can be rewritten as

$$|\langle E^i | H_r^F | E^f \rangle|^2 P_\beta(E) = \frac{\hbar}{2\pi e^2 R_T} f(E^i) [1 - f(E^f)], \quad (\text{S16})$$

where $f(E)$ represents the equilibrium Fermi-Dirac distribution.

Combining the fermionic and bosonic parts and including the phase factor $\exp[i(E^i - E^f + eV)t/\hbar]$, we arrive at the expression for the backscattering rate

$$\begin{aligned} \Gamma(V, T) &= \frac{1}{2\pi\hbar e^2 R_T} \int_{-\infty}^{\infty} dE^i dE^f f(E^i) [1 - f(E^f + eV)] \int_{-\infty}^{+\infty} dt e^{J(t)} e^{i(E^i - E^f)t} \\ &= \frac{1}{2\pi e^2 R_T} \frac{e^{\frac{eV}{2k_B T}}}{\Gamma(\frac{2}{1+r} + 2)} \left(\frac{2\pi k_B T}{\hbar\omega_R} \right)^{\frac{2}{1+r} + 1} \hbar\omega_R \left| \Gamma\left(\frac{1}{1+r} + 1 + i\frac{eV}{2\pi k_B T}\right) \right|^2. \end{aligned} \quad (\text{S17})$$

Physically, this rate only involves tunneling from the right-moving to left-moving channel. The net tunneling rate is described by the difference $\Gamma(V, T) - \Gamma(-V, T)$. Since the energy associated with the bias in each backscattering process is eV , we can reasonably argue that the charge carried by each quasi-particle is e . Consequently, the backscattering-related current is $\Delta I(V, T) = e[\Gamma(V, T) - \Gamma(-V, T)]$.

As a limiting case, we know from Eq. (S11) that when $A = 0$ the two fermionic chiral channels are decoupled, and the system attains a perfect conductance $G = e^2/h$. Thus we conclude that the current is

$$\begin{aligned} I(V, T) &= \frac{e^2}{h} V - \Delta I(V, T) \\ &= \frac{e^2}{h} V - e[\Gamma(V, T) - \Gamma(-V, T)] \\ &= \frac{e^2}{h} V - \frac{1}{R_T} \frac{1}{\Gamma(\frac{2}{1+r} + 2)} \left(\frac{2\pi k_B T}{\hbar\omega_R} \right)^{\frac{2}{1+r}} \times V \times \frac{|\Gamma(\frac{1}{1+r} + 1 + i\frac{eV}{2\pi k_B T})|^2}{|\Gamma(1 + i\frac{eV}{2\pi k_B T})|^2}, \end{aligned} \quad (\text{S18})$$

where we have used the equality $\sinh(\pi x) = \pi x \cdot 1/|\Gamma(1 + ix)|^2$. Eq. (S18) is exactly the current given in the main text [Eq. (21)].

-
- [S1] Alexander Altland and Ben Simons, *Condensed Matter Field Theory* (Cambridge University Press, Cambridge, 2006).
- [S2] A. Rosch, J. Paaske, J. Kroha, and P. Wölfle, "Nonequilibrium transport through a Kondo dot in a magnetic field: Perturbation theory and poor man's scaling," *Phys. Rev. Lett.* **90**, 076804 (2003).
- [S3] A. Rosch, J. Paaske, J. Kroha, and P. Wölfle, "The Kondo effect in non-equilibrium quantum dots: Perturbative renormalization group," *J. Phys. Soc. Jpn.* **74**, 118–126 (2005).
- [S4] C.-H. Chung, K. Le Hur, M. Vojta, and P. Wölfle, "Nonequilibrium transport at a dissipative quantum phase transition," *Phys. Rev. Lett.* **102**, 216803 (2009).
- [S5] H. T. Mebrahtu, I. V. Borzenets, H. Zheng, Yu. V. Bomze, A. I. Smirnov, S. Florens, H. U. Baranger, and G. Finkelstein, "Observation of Majorana quantum critical behavior in a resonant level coupled to a dissipative environment," *Nat. Phys.* **9**, 732–737 (2013), arXiv:1212.3857.
- [S6] G.-L. Ingold and Yu. V. Nazarov, "Charge tunneling rates in ultrasmall junctions," in *Single Charge Tunneling: Coulomb Blockade Phenomena in Nanostructures*, edited by H. Grabert and M. H. Devoret (Plenum, New York, 1992) pp. 21–107, and arXiv:cond-mat/0508728.
- [S7] Yu. V. Nazarov and Y. M. Blanter, *Quantum Transport: Introduction to Nanoscience* (Cambridge University Press, Cambridge, 2009).
- [S8] M. Sasseti and U. Weiss, "Transport of 1d interacting electrons through barriers and effective tunnelling density of states," *EPL (Europhysics Letters)* **27**, 311 (1994).
- [S9] W. Zheng, J. R. Friedman, D. V. Averin, S. Y. Han, and J. E. Lukens, "Observation of strong Coulomb blockade in resistively isolated tunnel junctions," *Sol. State Comm.* **108**, 839–843 (1998).